Characterization and Modeling of High-Voltage Field-Stop IGBTs

X. Kang, A. Caiafa, E. Santi, J.L. Hudgins, P.R. Palmer*
Department of Electrical Engineering
University of South Carolina
Columbia, South Carolina
*Department of Engineering
University of Cambridge
Cambridge, UK

Abstract— **The HVFS (High-Voltage Field-Stop) IGBT is a promising power device for high power applications thanks to the robust characteristics offered by the field-stop technology, which combines the inherent advantages offered by PT (punch-through) and NPT (non-punch-through) structures while overcoming the drawbacks of each structure. In this work an electrothermal physics-based model for the field-stop IGBT is developed. The model contains a detailed description of the field-stop layer and it is validated using experimental results for a commercial 1,200 V / 60 A field-stop IGBT over the entire temperature range specified in the data sheets. The validated model is then used to simulate a 6.5 kV field-stop IGBT. The simulation results are compared with experimental results published in the literature and good agreement is obtained.** *

Keywords—power semiconductors modeling, high voltage IGBT, field-stop IGBT, physics-based power semiconductor models

I. Introduction

In recent years, the fabrication of HVFS (High-Voltage Field-Stop) IGBTs makes it possible for this medium power device to enter the high-voltage and high-current application field as a good replacement of the primary power devices (GTOs, IGCTs etc). The investigation of the 6.5kV IGBT module's application in traction, industrial drive and pulse power fields [1]-[2] has shown the great potential of HVFS IGBT modules in the high-power fields. The key technology of HVFS IGBT is the introduction of field-stop concept, which combines the inherent advantages offered by PT (punch-through) and NPT (non-punch-through) structures while overcoming the drawbacks of each structure. The higher blocking voltage and lower overall loss offered by the new technology make FS IGBTs a new generation of devices. Therefore, it is necessary and beneficial to characterize and model the HVFS IGBT since only little research and no modeling on the robust device has been presented in the literature to date [3-7]. In section II the field-stop concept is briefly described.

In the past the authors have developed a physics-based electrothermal IGBT model that has proven accurate in modeling IGBT behavior in a wide temperature range [8-11]. In section III, an analytical description of the field-stop layer is presented. In section IV the necessary modifications to the physics-based model in order to incorporate the model of the field-stop layer are described. Section V presents experimental and simulation results for FS IGBTs. First, static and dynamic experimental results on a 1200V 60A field-stop IGBT are presented. The reduction in current tail at high voltages described in the literature as an advantage of the field-stop approach is verified experimentally.

The field-stop model is then validated comparing simulation and experimental results for inductive turn off at various temperatures. The model is also able to capture the current tail reduction effect at high voltages.

Finally, the validated model is applied to a 6.5kV HVFS IGBT. Since it proved impossible to acquire an actual sample of this new device at the present time, experimental switching waveforms published in the literature are used for comparison. Good agreement between simulation and experimental results is obtained.

II. The Field-Stop Concept

The characteristics of previous generation IGBTs have been greatly improved by innovations such as the buffer layer structure and the carrier lifetime reduction processing for PT IGBTs, as well as by geometry optimization allowing reduction of the wafer layer thickness for NPT IGBTs. However, there seems to be little room for further improvements due to the inherent drawbacks of the two structures. For PT IGBTs, the extremely high carrier concentration in the buffer layer causes undesired high turn-off current and losses, and the processing to reduce carrier lifetime results in a rather high forward voltage drop. On the other hand, in NPT IGBTs, which have the desired low carrier concentration in the base, a rather thick *n*- drift region is needed for voltage blocking. The thick *n*- drift region leads to higher static and dynamic losses.

The field-stop concept successfully overcomes the drawbacks of the two structures by vertically shrinking the NPT IGBT to a structure with a thin *n*- drift region, and inserting a low doped field-stop layer instead of the high-doped buffer layer used in the PT IGBT. As a result, the FS IGBT exhibits drastically reduced overall losses and better high-voltage performance. The cross sections of three IGBT structures are shown in Fig. 1.

The weakly doped field-stop layer in the FS IGBT gives a trapezoidal electric field distribution under forward blocking (typical in PT IGBTs), which is more desirable than the triangular electric field distribution typical of NPT IGBTs, because it allows a reduction of the drift region thickness for the same blocking voltage. Moreover, the

*This work was supported by the U.S. Office of Naval Research under Grant N00014-00-1-0131.

inherent advantages of the NPT structure of low-efficiency emitter and the high carrier lifetime are still maintained, since the field-stop layer only pins the electric field under forward blocking without reducing the p-emitter injection efficiency, unlike the injection efficiency reduction from the highly doped buffer layer in the PT structure.

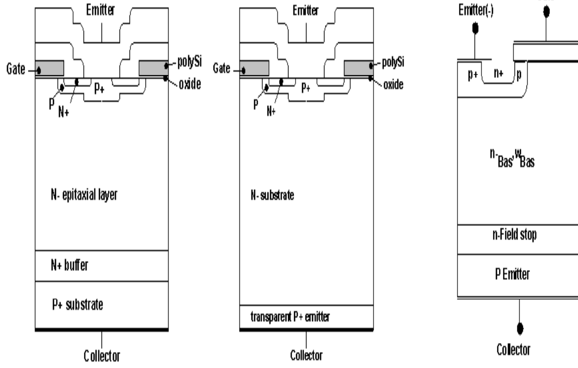

Fig. 1. Cross-section of PT IGBT (first), NPT IGBT (second) and FS IGBT (third).

III. Description of Field-Stop Layer

In order to develop a model for the FS IGBT, it is necessary to describe the field-stop layer (FSL). The behavior of the FSL is first described qualitatively and then a mathematical description of the FSL is given.

Fig. 2 defines some of the relevant variables used in this analysis. The addition of the buffer layer creates two junctions, the J_0 junction between the p+ emitter and the n doped FSL, and the J_1 junction between the FSL and the n-doped drift region. At junction J_0 there is a small electron current I_{n0} due to electron reverse injection into the p+ emitter. These electrons travel through the FSL coming from the drift region. Hole current I_{p0} injected from the p+ emitter travels mostly by diffusion through the FSL. Since the FSL is typically fairly thin in comparison with the field-stop diffusion length L_{pH}, there is little recombination in the FSL and most of the hole current reaches the drift region. This current, called I_{p1} in Fig. 2, represents hole injection from the FSL into the drift region. The component of hole current lost to recombination is compensated by an increase in the electron current, so that the electron current I_{n1} at junction J_1 is the sum of two terms: the recombination component plus the reverse injection electron current I_{n0}. The description so far applies to static conditions. Under dynamic conditions the additional hole current component due to variations in the stored charge in the FSL must be considered.

After this qualitative explanation, equations describing the FSL are introduced. The development follows the analysis of the buffer-layer IGBT given in [12-13]. The FSL equations given below are quasi-static, in the sense that they assume a steady-state carrier distribution in the FSL at all times. The capacitive effect related to variation in stored charge in the FSL is captured by adding a capacitive current term. The quasi-static approximation is justified by the fact that the FSL thickness is typically comparable to the diffusion length and the lifetime in the FSL is much shorter than in the drift region. On the other hand, the proposed model makes no such approximation in the wide drift region, where the ambipolar diffusion equation is solved directly, taking into account the distributed nature of charge transport [14].

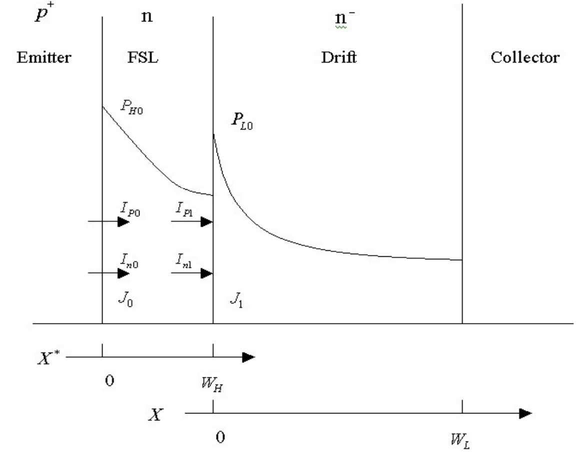

Fig. 2. Definition of various variables for FSL IGBT and typical carrier concentration in the various regions under forward conduction condition.

The symbols used are defined in the Nomenclature at the end of the paper. Assuming low-level injection in the FSL, in steady-state the excess hole concentration in the FSL is given by

$$\delta p(x) = \frac{P_{H0}\sinh(\frac{W_H - x}{L_{pH}}) + P_{HW}\sinh(\frac{x}{L_{pH}})}{\sinh(\frac{W_H}{L_{pH}})} \quad (1)$$

where P_{H0} and P_{HW} are the hole concentrations at the boundaries of the FSL. A typical excess hole concentration profile during conduction is shown in Fig. 2. Since the FSL thickness is comparable to a diffusion length, the profile is approximately linear.

Current continuity at the boundaries of the FSL requires that

$$I_A = I_{n0} + I_{p0} = I_{n1} + I_{p1} \quad (2)$$

where I_A is the anode current. Assuming quasi-equilibrium, the reverse injection current I_{n0} at junction J_0 is given by

$$I_{n0} = \frac{J_{sne} A N_H}{n_i^2} P_{H0} \quad (3)$$

where N_H is the doping concentration of the FSL and J_{sne} is the emitter electron saturation current density. This current component is usually small.

The hole current in the FSL is a minority current and therefore it is mostly diffusion current, so it can be expressed as

$$I_p = qAD_{pH}\frac{dp}{dx} \tag{4}$$

The hole current I_{p0} at the J_0 junction can be easily obtained by substituting the derivative of (1) for $x = 0$ into (4)

$$I_{p0} = \frac{qAD_{pH}}{L_{pH}\sinh(\frac{W_H}{L_{pH}})}[P_{H0}\cosh(\frac{W_H}{L_{pH}}) - P_{HW}] \tag{5}$$

Combining together equations (2), (3) and (5), the total current can be expressed as a linear combination of the hole concentrations at the boundaries of the FSL as

$$I_A = K_{PH0}P_{H0} - \frac{qAD_{pH}}{L_{pH}\sinh(\frac{W_H}{L_{pH}})}P_{HW} \tag{6}$$

where the constant K_{PH0} has been defined as

$$K_{PH0} = \left[\frac{J_{sne}AN_H}{n_i^2} + \frac{qAD_{pH}}{L_{pH}\tanh(\frac{W_H}{L_{pH}})}\right] \tag{7}$$

The hole current I_{p1} at the J_1 junction can be similarly obtained as

$$I_{p1} = \frac{qAD_{pH}}{L_{pH}\sinh(\frac{W_H}{L_{pH}})}[P_{H0} - P_{HW}\cosh(\frac{W_H}{L_{pH}})] + I_{QH} \tag{8}$$

The term I_{QH} represents the capacitive current due to variations in the charge Q_H stored in the FSL.

$$I_{QH} = -\frac{dQ_H}{dt} \tag{9}$$

Charge Q_H is approximately given by

$$Q_H = \frac{q(P_{H0} + P_{HW})AW_H}{2} \tag{10}$$

Finally the hole concentration P_{HW} at the boundary between the FSL and the drift region is given by

$$P_{HW} = \frac{{P_{L0}}^2}{N_H} \tag{11}$$

The voltage across junction J_0 is

$$V_{J0} = V_T \ln\left(\frac{P_{H0}N_H}{n_i^2}\right) \tag{12}$$

and the voltage across junction J_1 is

$$V_{J1} = V_T \ln\left(\frac{N_B}{P_{L0}}\right) \tag{13}$$

These equations are used in the proposed model to describe the effects of the FSL on the IGBT behavior as described in the following section.

IV. Implementation of FSL IGBT Model

The proposed FSL IGBT model is based on a model originally developed for NPT IGBT and described in [8-11]. This model solves directly the ambipolar diffusion equation in the drift region

$$D\frac{\partial^2 p(x,t)}{\partial x^2} = \frac{p(x,t)}{\tau} + \frac{\partial p(x,t)}{\partial t} \tag{14}$$

utilizing a Fourier series solution as proposed in [14]. The boundary conditions needed to compute the solution are the gradients of the carrier concentrations at the edges x_1 and x_2 of the drift region, which are given by

$$f(t) = \left[\frac{\partial p(x,t)}{\partial x}\right]_{x1} = \frac{1}{2qA}\left[\frac{I_{n1}}{D_n} - \frac{I_{p1}}{D_p}\right] \tag{15}$$

$$g(t) = \left[\frac{\partial p(x,t)}{\partial x}\right]_{x2} = \frac{1}{2qA}\left[\frac{I_{n2}}{D_n} - \frac{I_{p2}}{D_p}\right] \tag{16}$$

Therefore, in order to establish the boundary conditions, hole and electron currents at the edges of the drift region are needed. Since by current continuity it is

$$I_A = I_{n1} + I_{p1} = I_{n2} + I_{p2} \quad (17)$$

the sum of the hole and electron concentrations is known, so that it is sufficient to find one current component at each edge. For example at the MOS-channel edge the electron current I_{n2} is the channel current and it can be found as a function of the gate-cathode voltage using the well-known MOSFET equation. Current I_{p2} can then be calculated using (16). This boundary condition is not affected by the presence of the FSL and is the same as in the original NPT IGBT model.

On the other hand, the boundary condition at junction J_1 is affected by the FSL. Equivalently, one may say that the FSL affects the charge injection at junction J_1. For the NPT IGBT the boundary condition currents are

$$I_{n1} = qAh_p p_{L0}^2 \quad (18)$$

$$I_{p1} = I_A - I_{n1} \quad (19)$$

where h_p is the recombination parameter at the p+ layer [15]. For the FSL IGBT the boundary condition currents are found using the equations of the previous section as follows:

- Carrier concentration P_{HW} is calculated using (10).
- Carrier concentration P_{H0} is calculated solving (6) for P_{H0}

$$P_{H0} = \frac{I_A}{K_{PH0}} + \frac{qAD_{pH}}{K_{PH0} L_{pH} \sinh(\frac{W_H}{L_{pH}})} P_{HW} \quad (20)$$

- Capacitive current I_{QH} is calculated using (8) and (9).
- Current I_{p1} is calculated using (7).
- Current I_{n1} is calculated using (2).

This is the main change in the model to take into account the FSL. The only other change is that equations (11), (12) are used to find the junction voltage drops.

V. Experiment and Simulation

A 1200V/60A trench-gate FS IGBT was tested in this work. The static and dynamic testing were performed within the device operating temperature range from –50 to 125 ^oC. The dynamic experiments were performed at various temperatures under resistive hard switching conditions and clamped inductive hard switching conditions. The electrothermal PSpice FS-IGBT model described above was used in simulating the device switching behavior. For space reasons the paper focuses on the turn-off transient behavior, comparing simulation and experimental results.

A. *Field-Stop IGBT Experiment*

The static characteristic testing, including the forward drop and breakdown voltage, was performed with a standard curve tracer. The forward drop variation with temperature is shown in Fig. 3, where a positive forward drop temperature coefficient is shown. This static characteristic is similar to that of typical PT IGBTs and it shows that the FS IGBT is suitable for applications requiring paralleling of discrete devices and for multi-chip modules.

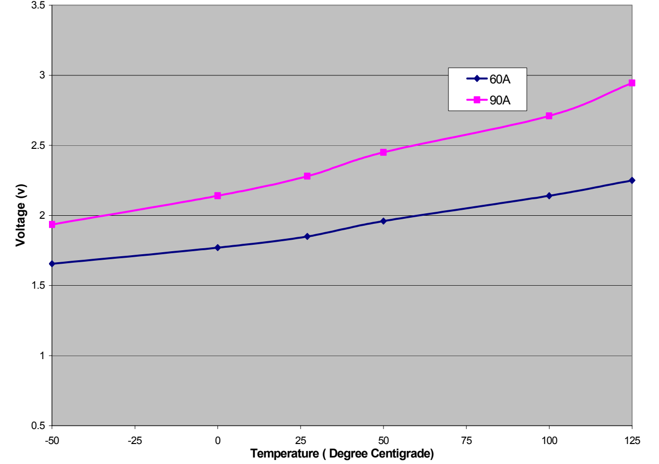

Fig. 3. FS IGBT Forward drop variation with temperatures.

The static test also showed that the device breakdown voltage decreases at low temperature from 1400V at or above ambient temperature to 1200V at -50 ^oC. The decrease in breakdown voltage, which was also observed in NPT and PT IGBTs in former experiments by the authors, is strongly related to the silicon design. It is also conceivable that the breakdown-dominating component is the anti-paralleling diode inside the device, instead of the IGBT itself.

In order to minimize the external circuit effect on the IGBT characteristics, resistive switching tests were conducted in addition to the standard inductive load testing. The circuit diagrams are shown in Fig 4. In order to perform the thermal test, the device was placed inside an environmental chamber.

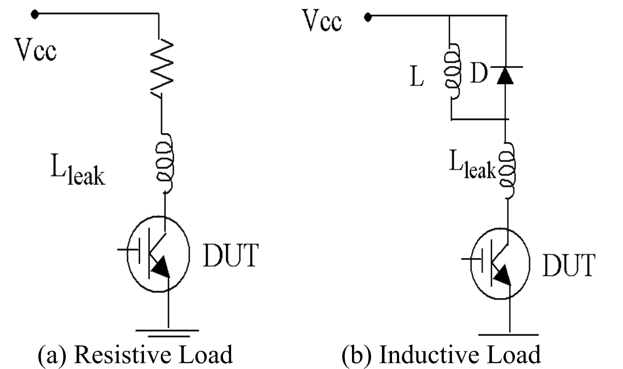

Fig. 4. FS IGBT testing Circuit.

The measurements of IGBT turn-off transient under these two circuit conditions were performed at 600 V supply

voltage and 60 A collector current under the same gate conditions. Fig. 5 and 6 respectively show the IGBT falling current variation at turn off at temperatures from –50 to 125 ^{o}C.

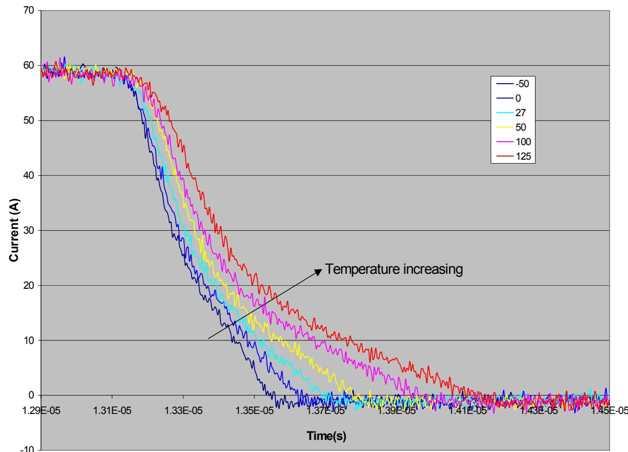

Fig. 5. Family of curves showing collector current fall during IGBT turn-off in the resistive load circuit at various temperatures. The peak current is 60A. The horizontal scale is 200ns/div.

Because of the positive temperature coefficient of the lifetime, the turn-off current waveform changes significantly with temperature under both circuits conditions, becoming slower with increasing temperature. Comparison of the two figures also shows that typical 2-stage collector current waveform during IGBT turn-off is very obvious under inductive switching conditions, but it is less obvious under resistive load conditions. This is due to the fact that under resistive switching conditions the voltage rise and the current fall happen simultaneously, whereas under inductive switching conditions the collector voltage rise takes place at constant current and the current starts decreasing only later on when the diode becomes forward biased.

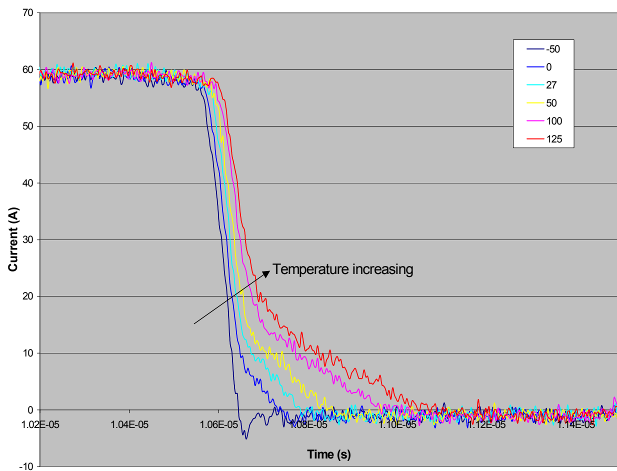

Fig. 6. Family of curves showing collector current fall during IGBT turn-off in the clamped inductive load circuit at various temperatures. The peak current is 60A. The horizontal scale is 200ns/div.

Considering the above differences and the importance of inductive switching in practical converter applications, further measurements and simulations of FS IGBT turn-off transient were performed with the clamped inductive circuit.

It is known that the current tail of buffer-layer and field-stop IGBTs at turn-off changes significantly with turn-off voltage. In particular the current tail decreases at higher collector-emitter voltages, so that turn-off losses are reduced. This is due to the fact that the lifetime in the buffer layer is significantly smaller than the lifetime in the low-doped drift region, and at high voltages when the depletion layer increases the buffer layer makes up a bigger portion of the undepleted base. This effect is investigated experimentally by performing FS IGBT turn off under different collector-emitter voltage conditions. Fig. 7 shows the variation of the total current fall time and current tail time at voltages from 300 V to 900 V.

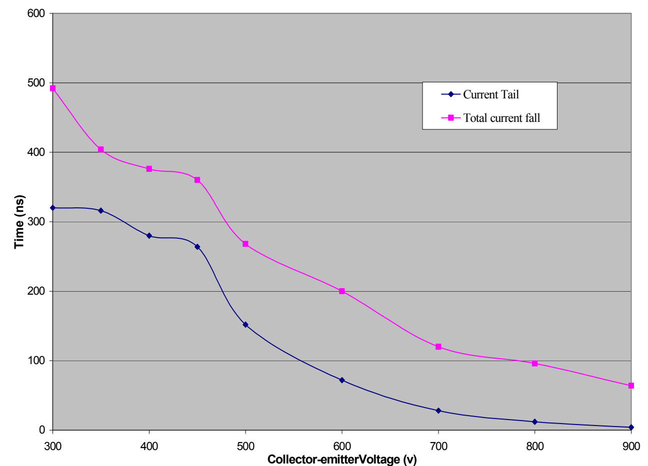

Fig 7. Collector current fall variation with different collector-emitter voltages. The horizontal scale is 100 volts/div and the vertical scale is 100ns/div.

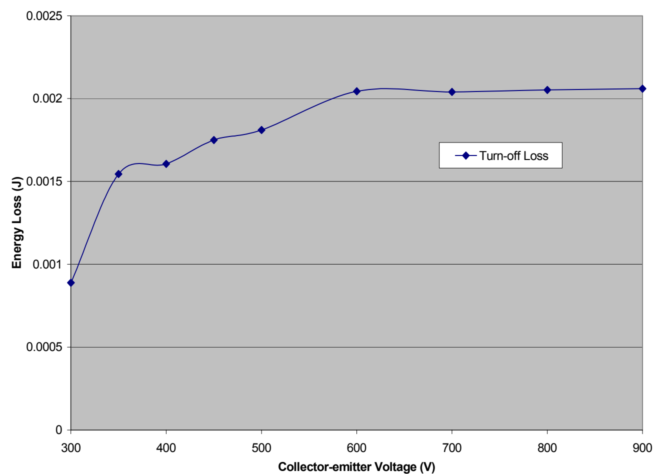

Fig 8. Turn off energy loss variation with different collector-emitter voltages. The horizontal scale is 100 volts/div.

The results show that the tail current duration is greatly reduced when the collector-emitter voltage is large, so that the electric field reaches or almost reaches the field-stop layer.

Fig. 8 shows turn-off losses as a function of voltage. At low voltages losses increase with voltage as one would expect in a conventional NPT IGBT. However at higher voltages turn-off losses are approximately constant due to the reduction in current tail duration.

B. *Comparison of Experiment and Simulation*

The PSpice physics-based model described in the prior section has been used to simulate the FS IGBT turn-off switching behavior in the clamped inductive circuit.

Most parameters of the model can be directly obtained from the datasheet or easily extracted with static testing, such as the MOS gate parameters. The extraction of other parameters of the *n*- drift region and FSL are mainly based on [12-13]. Typical values were chosen for the FSL parameters: the doping concentration is around $10^{15} \sim 10^{16}$ cm^{-3}, the FSL width is around 8 ~ 10 μm for the 1200V device. The detailed parameterization procedure will be given in a future work.

The comparison between experiment and simulation results at various temperatures: 27 °C, -50 °C and 100 °C is shown in Fig. 9-11, respectively. The collector-emitter voltage is 600 V, and the current is 60 A. In each figure, the simulation curves were intentionally shifted forward by 20ns for legibility, and the horizontal scale is 200ns/div. The good match shown in the figures strongly demonstrates the accuracy and robustness of the model.

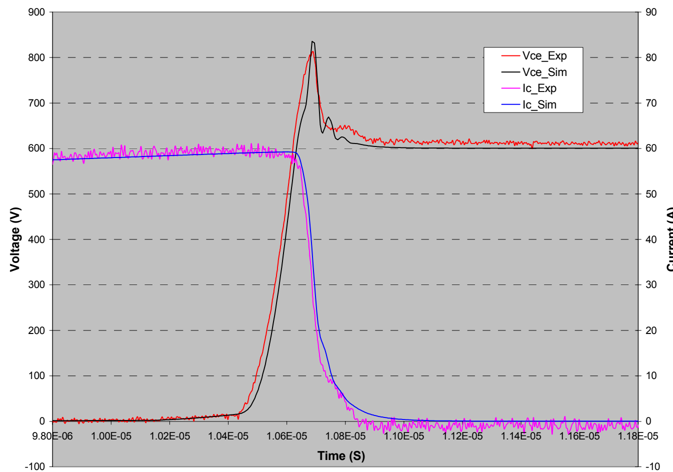

Fig. 9 . Comparison between the experimental result (red-voltage & pink-current) and simulation (black-voltage & blue-current) during turn-off at 27 °C.

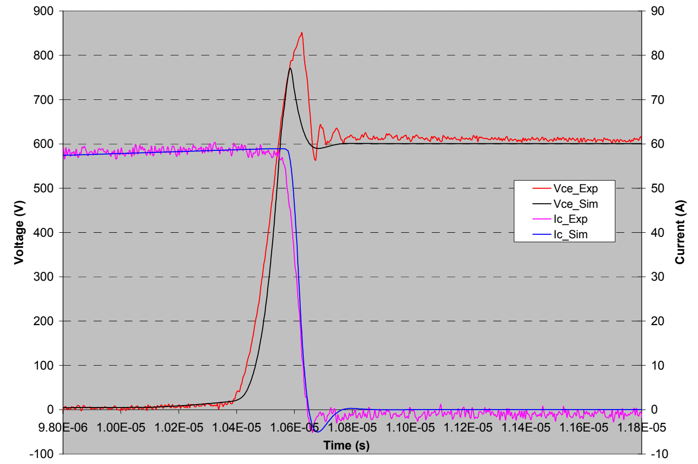

Fig. 10. Comparison between the experimental result (red-voltage & pink-current) and simulation (black-voltage & blue-current) during turn-off at -50 °C.

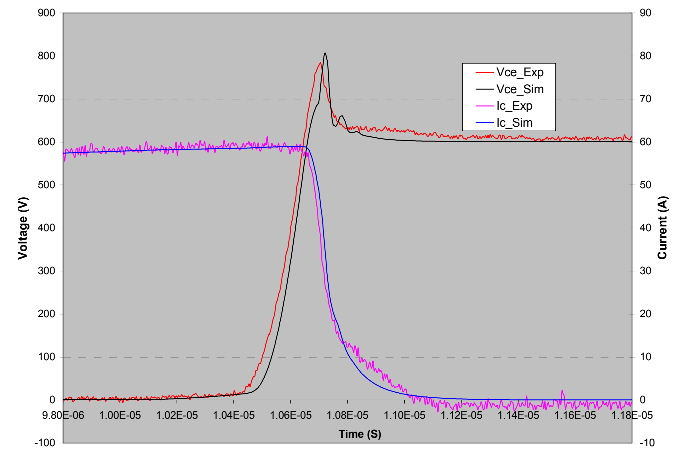

Fig. 11 . Comparison between the experimental result (red-voltage & pink-current) and simulation (black-voltage & blue-current) during turn-off at 100 °C.

Beside the accurate thermal simulation of FS IGBT turn-off, the reduction of current tail at higher voltages in field-stop IGBTs was also successfully simulated with the model. The simulation of the turn off under 900 V collect-emitter voltage and 60 A collector current is shown in Fig. 12. The current waveform should be compared with the one in Fig. 9, showing the dramatic reduction in current tail.

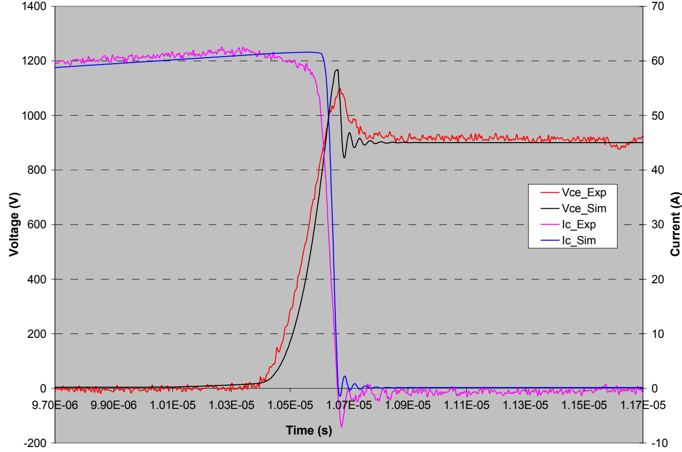

Fig. 12 . Comparison between the experimental result (red-voltage & pink-current) and simulation (black-voltage & blue-current) during turn-off at 900V collector-emitter voltage and 60A current at 27 °C.

C. *Simulation of 6.5KV FS IGBT*

In this work, the FS IGBT model was also used to simulate the new 6.5kV HVFS IGBT turn-off behavior. Due to the impossibility to obtain samples, the experimental waveform of the high voltage FS IGBT was extracted from figure 3 of [3] using a curve-fitting software tool and Matlab.

Fig. 13 shows the comparison of the curve-fitting waveform and simulation of the 6.5KV FS IGBT turn off at 4400V collector-emitter voltage and 1200A collector current. The horizontal division in the figure is 2us/div.

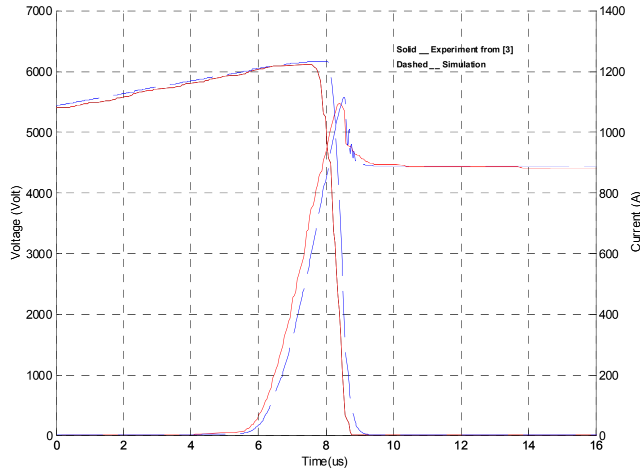

Fig. 13 . Comparison between the experimental data from [3] (red solid curves) and simulation (blue dashed) during the turn-off.

The good match proves one more time that the physics-based model is robust enough to simulate high voltage FS IGBT.

VI. Discussion and Conclusions

Based on the previous work of the NPT and PT IGBTs, the paper successfully develops the FS IGBT model using a quasi-static description of the *n* doped field-stop layer. The model is based on a Fourier series solution of the ambipolar diffusion equation in the drift region, accurately describing the distributed nature of charge transport in the drift region.

The static testing and hard switching experiment with FS IGBT confirm the advantages of the field-stop concept. The good agreement between the experiment and simulation results further validates the approach and confirms the robustness of the model.

Results from the validated model are compared with published results for a 6.5kV HVFS IGBT , showing good agreement. This shows that the model is indeed capable of predicting the behavior of HVFS IGBTs.

VII. Nomenclature

FSL	Field-stop layer.
$J0$	Junction between emitter and FSL.
$J1$	Junction between FSL and drift region.
$J2$	Junction between drift region and *p*+ body.
n, p	Electron, hole carrier concentration (cm^{-3}).
δp	Excess hole concentration (cm^{-3}).
P_{L0}	δp at field-stop edge of drift region (cm^{-3}).
P_{H0}	δp at emitter edge of FSL (cm^{-3}).
P_{HW}	δp at field-stop edge of drift region (cm^{-3}).
W_H	Width of FSL (μm).
Q_H	Excess charge in FSL (C).
h_p	Recombination parameter at the *p*+ layer (1/s cm^2).
L_{pH}	Hole diffusion length in FSL (μm).
I_A	Total current (A).
I_{n0}, I_{p0}	Electron and hole currents at junction J_0 (A).
I_{n1}, I_{p1}	Electron and hole currents at junction J_1 (A).
I_{n2}, I_{p2}	Electron and hole currents at junction J_2 (A).
I_{QH}	Capacitive current (A).
J_{sne}	Emitter electron saturation current density (A/cm^2).
A	Device cross-section (cm^3).
q	Electronic charge ($1.6x10^{-19}$ C).
D_{pH}	Hole diffusivity in FSL (cm^2/s).
V_{J0}	Voltage across junction J_0 (V).
V_{J1}	Voltage across junction J_1 (V).
D	Ambipolar diffusivity in drift region (cm^2/s).
D_n, D_p	Electron, hole diffusivity (cm^2/s).
τ	High carrier level lifetime in drift region (μs).

REFERENCES

[1] T. Laska, M. Matschitsch and W.Scholz, "Ultrathin-wafer Technology for a new 600V-NPT_IGBT," Proceeding of the 9th ISPSD, 1997, pp.361-364

[2] M. Hierholzer, T. Laska, M.Munzer, F.Pfirsch, C.Schaffer and T.Schmidt, "3rd Generation of 1200V IGBT Modules," *PCIM Proceedings,* 1999, pp. 221-226.

[3] T. Schuetze, H. Berg, O. Schilling, "6.5kV IGBT Module Delivers Reliable Medium-Voltage Performance—Part 1: Electrical," *PCIM,* August 2001, pp. 14-18.

[4] T. Schuetze, H. Berg, O. Schilling, "6.5kV IGBT Module Delivers Reliable Medium-Voltage Performance—Part 2: Packaging," *PCIM,* September 2001, pp. 39-46.

[5] T. Laska, M.Munzer, F.Pfirsch, C.Schaeffer and T.Schmidt, "The Field Stop IGBT(FS IGBT) – A New Power Device Concept with a Great Improvement Potential," *ISPSD'2000,* May 22-25,Toulouse, France, pp. 355-358.

[6] J.G.Bauer, F.Auerbach, A.Porst and R.Roth etc. "6.5kV-Modules using IGBts with Field Stop Technology," *ISPSD'2001,* Osaka, pp. 121-124.

[7] O.Schilling, D.Scholz and H.Seidelmann etc. "6.5kV Pree Pack IGBT for High Power Application," PCIM 2001.

[8] P.R. Palmer, J.C. Joyce, P.Y. Eng, J.L. Hudgins, E. Santi, and R. Dougal, "Circuit simulator models for the diode and IGBT with full temperature dependent features," *IEEE PESC Rec.,* pp. , June 2001.

[9] E. Santi, A. Caiafa, X. Kang, J.L. Hudgins, P.R. Palmer, D. Goodwine, and A. Monti "Temperature effects on trench-gate IGBTs," *IEEE IAS Annual Mtg. Rec.*, Oct. 2001.

[10] X. Kang, A. Caiafa, E. Santi, J.L. Hudgins and P.R. Palmer "Parameter Extraction for a Power Diode Circuit Simulator Model Including Temperature Dependent Effects," *IEEE APEC Annual Mtg. Rec.*, March. 2002.

[11] X. Kang, A. Caiafa, E. Santi, J.L. Hudgins and P.R. Palmer "Low Temperature Characterization and Modeling of IGBTs," *IEEE PESC Annual Mtg. Rec.*, in press, June. 2002.

[12] A.R. Hefner Jr. and D.L. Blackburn, "A performance trade-off for the insulated gate bipolar transistor: buffer layer versus base lifetime reduction", *IEEE Trans.P.E* , vol. 2, no. 3, pp. 194-206, 1987.

[13] A.R. Hefner Jr., "Modeling buffer layer IGBT's for circuit simulation", *IEEE Trans.P.E* , vol. 10, no. 2, pp. 111-123, 1995.

[14] Ph. Leturcq, M.O. Berraies and J.L Massol "Implementation and Validation of a New Diode Model for Circuit Simulation" *IEEE PESC Rec.* 1996

[15] H. Schlangenotto and W. Gerlach, "On the effective carrier lifetime in *p-s-n* rectifiers at high injection levels," *Solid-State Electronics*, vol. 12, pp. 267-275, 1969.